J Solid State Electrochem (2012) 16:2797–2804
DOI 10.1007/s10008-012-1702-y

ORIGINAL PAPER

Electrochemical evaluation of $La_2NiO_{4+\delta}$-based composite electrodes screen-printed on $Ce_{0.8}Sm_{0.2}O_{1.9}$ electrolyte

Kai Zhao · Qing Xu · Duan-Ping Huang · Min Chen · Bok-Hee Kim

Received: 15 December 2011 / Revised: 18 February 2012 / Accepted: 22 February 2012 / Published online: 8 March 2012

Abstract $La_2NiO_{4+\delta}$, 60 wt.% $La_2NiO_{4+\delta}$–40 wt.% $La_{0.6}Sr_{0.4}Co_{0.2}Fe_{0.8}O_{3-\delta}$, and 60 wt.% $La_2NiO_{4+\delta}$–40 wt.% $Ce_{0.8}Sm_{0.2}O_{1.9}$ electrodes were prepared from fine powders on dense $Ce_{0.8}Sm_{0.2}O_{1.9}$ electrolyte substrates by screen-printing technique. Electrochemical impedance spectroscopy and chronopotentiometry techniques were employed to evaluate the electrochemical properties of the composite electrodes in comparison with the $La_2NiO_{4+\delta}$ electrode. For the three electrodes, main electrode processes were resolved to be charge-transfer at the electrode/electrolyte interface and oxygen exchange on the electrode surface. The contribution of the surface oxygen exchange process was detected to be dominant for the overall electrode polarization. The addition of $Ce_{0.8}Sm_{0.2}O_{1.9}$ into $La_2NiO_{4+\delta}$ was favorable for the charge transfer process whereas it was undesired for the surface oxygen exchange process. On comparison, adding $La_{0.6}Sr_{0.4}Co_{0.2}Fe_{0.8}O_{3-\delta}$ into $La_2NiO_{4+\delta}$ was found to benefit both the two electrode processes. The $La_2NiO_{4+\delta}$-$La_{0.6}Sr_{0.4}Co_{0.2}Fe_{0.8}O_{3-\delta}$ composite electrode showed optimum electrochemical properties among the three electrodes. At 800 °C, the composite electrode achieved a polarization resistance of 0.20 Ω cm^2, an overpotential of 45 mV at a current density of 200 mA cm^{-2}, together with an exchange current density of ~200 mA cm^{-2}.

Keywords $La_2NiO_{4+\delta}$ · $La_{0.6}Sr_{0.4}Co_{0.2}Fe_{0.8}O_{3-\delta}$ · $Ce_{0.8}Sm_{0.2}O_{1.9}$ · Composite electrode · Polarization

K. Zhao · M. Chen · B.-H. Kim
Division of Advanced Materials Engineering, Hydrogen & Fuel Cell Research Center, Chonbuk National University, Jeonju 561-756, South Korea

K. Zhao · Q. Xu (✉) · D.-P. Huang
School of Materials Science and Engineering, Wuhan University of Technology, Wuhan 430070, People's Republic of China
e-mail: xuqing@whut.edu.cn

Present Address:
M. Chen
Department of Chemistry, University of Calgary, 2500 University Drive NW, Calgary, AB T2N1N4, Canada

Introduction

Solid oxide fuel cells (SOFCs) are energy conversion devices with high efficiency and environmental advantages. In the past decades, there has been a continuous effort to reduce the operation temperature of SOFCs down to intermediate temperatures (600–800 °C) or less. One of the major problems encountered at reduced operation temperatures is increase in the polarization loss from the cathodes. This leads to a performance degradation of the intermediate temperature SOFCs (IT-SOFCs) [1]. Due to extended electrochemical reaction region, adopting electronic–ionic mixed conductors as the cathode is a feasible way to solve the problem. This promoted cathodic reaction kinetics at the intermediate temperatures. Extensive researches have been conducted to develop novel mixed conducting electrode materials with desirable overall properties. Recently, layer-structured $Ln_2NiO_{4+\delta}$-based compounds emerged as a promising candidate material for the cathode of IT-SOFCs. This is due to their high oxygen diffusion and surface exchange

coefficients at the intermediate temperatures coupled with moderate thermal expansion coefficients around 13.0×10^{-6} K^{-1} [2, 3]. Among them, $La_2NiO_{4+\delta}$ (LN) has drawn much attention by its virtue of satisfactory stability over wide ranges of temperature and oxygen partial pressure [4].

In many cases, cathodic polarization of a SOFC device accounts for a dominant part of the whole cell polarization [5]. Therefore, electrocatalytic activity towards oxygen reduction is an important criterion to evaluate the application potential of a cathode in SOFC devices. The electrochemical properties of $Ln_2NiO_{4+\delta}$-based mixed conductors have been extensively inspected in view of the application of IT-SOFCs as the cathode [6–10]. The kinetics of oxygen reduction reaction on the surface of $Ln_2NiO_{4+\delta}$-based cathodes has been investigated. This is done by the electrochemical impedance spectroscopy (EIS) technique under various direct-current (DC) bias conditions and/or oxygen partial pressures [11–15]. Moreover, the performance of $Ln_2NiO_{4+\delta}$-based cathodes has been assessed based on single-cell devices [5, 9, 15].

The electronic and oxygen-ionic conductivities of a mixed conducting cathode material act as the intrinsic contributing factors to the electrochemical properties of the cathode [16]. Hence, the role of electronic and oxygen-ionic conducting components in the electrocatalytic activity is an intriguing topic with practical importance. Perovskite-type $La_{0.6}Sr_{0.4}Co_{0.2}Fe_{0.8}O_{3-\delta}$ (LSCF) exhibits high electronic conductivity with the order of magnitude of about 10^2 S cm^{-1} and appreciable oxygen-ionic conductivity at the intermediate temperatures [17]. On the other hand, fluorite-type $Ce_{0.8}Sm_{0.2}O_{1.9}$ (SDC) has been recognized as a superior intermediate-temperature oxygen-ionic conductor (10^{-2} S cm^{-1}) [18]. Despite extensive researches on the electrochemical properties of $Ln_2NiO_{4+\delta}$-based cathodes, research effort towards composite electrodes composed of layer-structured compounds together with the LSCF or SDC remains rather limited. Gaining more insight into the electrochemical properties of the composite electrodes is expected to provide useful information regarding the effect of the electronic and oxygen-ionic conducting components. Such information may, in turn, lead to a guideline for the development of novel cathode materials with high electrocatalytic activity.

We prepared the LN, LN-LSCF, and LN-SDC electrodes on the SDC electrolyte substrates by screen-printing technique. In this work, we study the electrochemical properties of the composite electrodes in comparison with the LN electrode.

Experimental

LN powder was synthesized by a polyaminocarboxylate complex precursor method. Reagent-grade $La(OH)_3$ (99.5 %, Yutaixian Qingda Fine Chemical Factory, China), $NiCO_3{\cdot}2Ni(OH)_2{\cdot}4H_2O$ (99.4 %, Shanghai Guanghua Technology Co., Ltd., China), and diethylenetriaminepentaacetic acid (99.0 %, Sinopharm Chemical Reagent Co., Ltd., Shanghai, China) were used as starting materials. The starting materials were dissolved into deionized water and stirred to form a transparent aqueous solution. The solution was then heated to yield a solid polyaminocarboxylate complex. The solid complex precursor was pulverized and calcined at 900 °C for 2 h in air. X-ray diffraction (XRD) analysis for the calcined powder identified the formation of a pure K_2NiF_4 phase. The detail of the synthesis process has been described elsewhere [19]. LSCF powder was synthesized by a glycine–nitrate combustion process (GNP). Reagent-grade $La(NO_3)_3{\cdot}6H_2O$ (99.0 %), $Sr(NO_3)_2$ (99.5 %), $Co(NO_3)_3{\cdot}6H_2O$ (99.0 %), $Fe(NO_3)_3{\cdot}9H_2O$ (98.5 %), and glycine (99.5 %) (Sinopharm Chemical Reagent Co., Ltd., Shanghai, China) were used as starting materials. The starting materials were dissolved into deionized water to form a solution and then, heated on a hot plate until auto-igniting combustion occurred. To ensure a pure perovskite phase, the combusted powder was calcined at 700 °C. The GNP combustion synthesis of the powder has been previously reported [20]. SDC powder was synthesized by a urea-combustion method. Reagent-grade $Ce(NO_3)_3{\cdot}6H_2O$ (99.0 %), $Sm(NO_3)_3{\cdot}6H_2O$ (99.0 %), and urea ($CO(NH_2)_2$) (99.0 %) (Sinopharm Chemical Reagent Co., Ltd., Shanghai, China) were used as starting materials. The starting materials were dissolved into the deionized water to form a solution and then were heated on a hot plate to ignite a self-sustaining combustion. XRD analysis certified that the combusted powder had a pure cubic fluorite phase. The SDC powder was compacted into disks of 17 mm in diameter and then sintering at 1,300 °C for 4 h in air. The SDC ceramic specimens attained over 96 % of theoretical density. The preparation of SDC powder and ceramics has been reported in an earlier paper [21].

Three-electrode electrochemical cells were prepared employing the LN, 60 wt.% LN–40 wt.% LSCF, and 60 wt.% LN–40 wt.% SDC as the electrode, respectively. Figure 1 schematically shows the configuration and geometrical parameters of the cells. By a screen-printing technique, the electrodes were prepared onto dense SDC substrates. Taking into consideration the percolation of the constituents, weight fractions of the LSCF and the SDC in the composite electrodes were determined [22]. The powders were mixed with organic solution at a solid loading of 70 wt.% to form a slurry-like ink. The organic solution was composed of 9 wt.% ethyl cellulose (99.0 %), 10 wt.% dibutyl phthalate (99.5 %), 10 wt.% butyl alcohol (99.0 %), and 71 wt.% terpineol (99.0 %) (Sinopharm Chemical Reagent Co., Ltd., Shanghai, China). The LN and LN-LSCF electrodes were sintered at 950 °C. The sintering temperature of the LN-SDC electrode was elevated to 1,000 °C. This is done to ensure a satisfactory adhesion between the electrode and the electrolyte substrate.

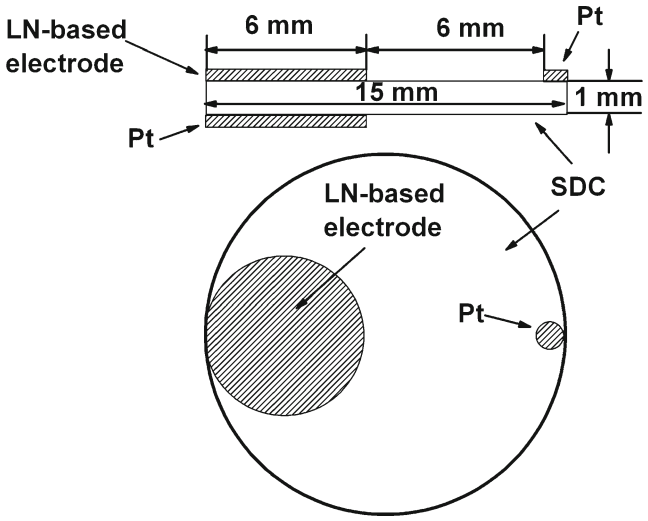

Fig. 1 Schematic diagram and geometrical parameters of the three-electrode electrochemical cells

Platinum paste was painted as the counter and reference electrodes, respectively. Platinum mesh was applied on the top of the working electrode as the current collector.

The morphology of the powders and the microstructure of the cells were investigated by a JEOL JSM 5610LV scanning electron microscope (SEM). The particle size of the powders and grain size of the electrodes were determined from the image analysis method using the Image Profession Plus software. The porosity of the electrodes was estimated based on counting the black and gray pixels in the SEM micrographs, which refer to pores and grains, respectively [23]. The electrochemical properties of the electrodes were measured at a CHI 660 C electrochemical work station. The electrochemical impedance spectra of the electrochemical cells were measured under zero DC bias in the frequency range of 0.01 Hz to 100 kHz. The amplitude of the input sinuous signals was 5 mV. Using the Zview 3.1a software, the measured data were analyzed. DC polarization was measured by chronopotentiometry technique with 25 current density steps from 10 to 250 mA cm^{-2}. The polarization current was applied step by step between the working and the counter electrodes. For each step, the voltages between the working and reference electrodes were recorded as a function of time until the potential of the working electrode reached a steady state. The cathodic overpotential was calculated according to the following equation [12]:

$$\eta_{\mathrm{WR}} = \Delta U_{\mathrm{WR}} - I \cdot \mathrm{R}_{el} \quad (1)$$

where, η_{WR} represents the cathodic overpotential, ΔU_{WR} is the voltage between the working and the reference electrodes, I is the applied current flowing through the cell, and R_{el} is the ohmic resistance determined from the EIS measurement.

Results and discussion

Figure 2 shows the SEM micrographs of the LN, LSCF, and SDC powders. The powders consisted of fine and homogeneous particles with weak agglomeration. The average particle sizes of LN, LSCF, and SDC powders were determined to be 100±10, 60±10, and 60±10 nm, respectively.

Figure 3 shows the SEM micrographs of the LN, LN-LSCF, and LN-SDC electrodes. Each electrode displayed a porous feature, a good adhesion to the electrolyte substrate, and basically a uniform thickness. The thicknesses of the electrodes slightly varied in the range of 13 to 17 μm. The average grain sizes and porosities of the electrodes were estimated to be around 200 nm and 10 %, respectively. In general, no significant difference in microstructure could be found out for the three electrodes.

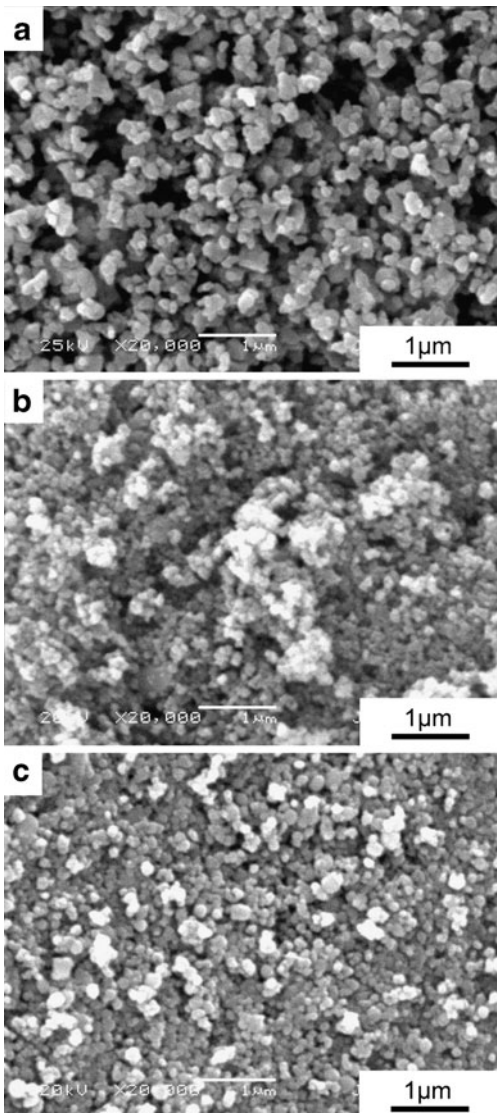

Fig. 2 SEM micrographs of **a** LN, **b** LSCF, and **c** SDC powder

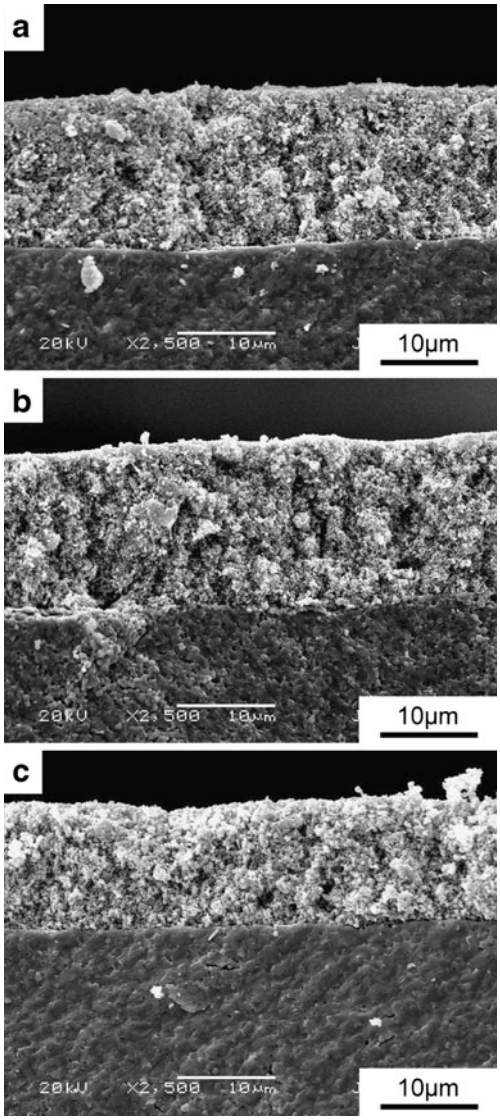

Fig. 3 SEM micrographs of **a** LN, **b** LN-LSCF, **c** LN-SDC electrodes

Figure 4 shows the Nyquist plots of the LN, LN-LSCF, and LN-SDC electrodes measured at different temperatures. Inductive impedance responses were detected at each temperature. They appeared as a high-frequency tail below the real axis. As is well known, the inductive impedance responses were caused by the measurement device and connecting wires [4]. Thus, these impedance responses were subtracted from the spectra [24]. The Nyquist plots measured at different temperatures are obviously asymmetric in shape, implying more than one electrode process. The impedance spectra were fitted according to an $R_{el}(R_1Q_1)(R_2Q_2)(R_3Q_3)$ equivalent circuit model. The (RQ) components correspond to the involved electrode processes. For the (RQ) components, R is the resistance and Q is the constant phase element. The impedance Z_Q of a constant phase element Q and equivalent capacitance C of the (RQ) components can be calculated according to the following equations [25]:

$$Z_Q = \frac{1}{Q(i\cdot\omega)^n} \tag{2}$$

$$C = \frac{(R\cdot Q)^{1/n}}{R} \tag{3}$$

where, ω is the angular frequency and n is an exponent. The constant phase element Q represents an ideal capacitor and an ideal resistor when $n=1$ and $n=0$, respectively. When $0<n<1$, the circuit component reflects inhomogeneity of the electrode system. The relaxation frequency f of an electrode process corresponding to a specific (RQ) component can be calculated by the following equation [25]:

$$f = \frac{(R\cdot Q)^{-1/n}}{2\pi} \tag{4}$$

From Fig. 4, it can be seen that the fitting results agree well with the experimental data. Table 1 lists the parameters of the circuit elements which are derived from spectrum fitting. The parameters were normalized with the geometrical factors of the cells.

The equivalent capacitance and relaxation frequency can be applied as characteristic parameters to identify the electrode processes. The assignation of the electrode processes involved in the present work was ascertained by comparing our parameters with literature results. The electrode process corresponding to the component (R_1Q_1) had the equivalent capacitances of 10^{-6}–10^{-5} F cm^{-2} and the relaxation frequencies of 10^4–10^6 Hz. Thus, the electrode process is attributed to the charge transfer process of oxygen ions between the electrode and electrolyte [13, 26]. The electrode processes corresponding to the components (R_2Q_2) and (R_3Q_3) showed the equivalent capacitances of 10^{-4} and 10^{-3} F cm^{-2} along with the relaxation frequencies of 10–10^4 and 10–10^2 Hz, respectively. Accordingly, the former process is assigned to the electron transfer between oxygen and the electrodes, while the latter one is ascribed to the adsorption and dissociation of molecular oxygen on the surface of the electrodes. Both these processes can be classified as the steps for oxygen exchange on the surface of the electrodes [27–29]. For each electrode, the polarization resistance originating from the surface oxygen exchange process acted as a major contribution to the overall electrode polarization resistance (R_p). This suggests a critical role of the process in the overall electrode reaction. For each electrode reaction process, the data of the relaxation frequency and measurement temperature basically fitted with the Arrhenius relation (not shown here). This is in agreement with literature results [13].

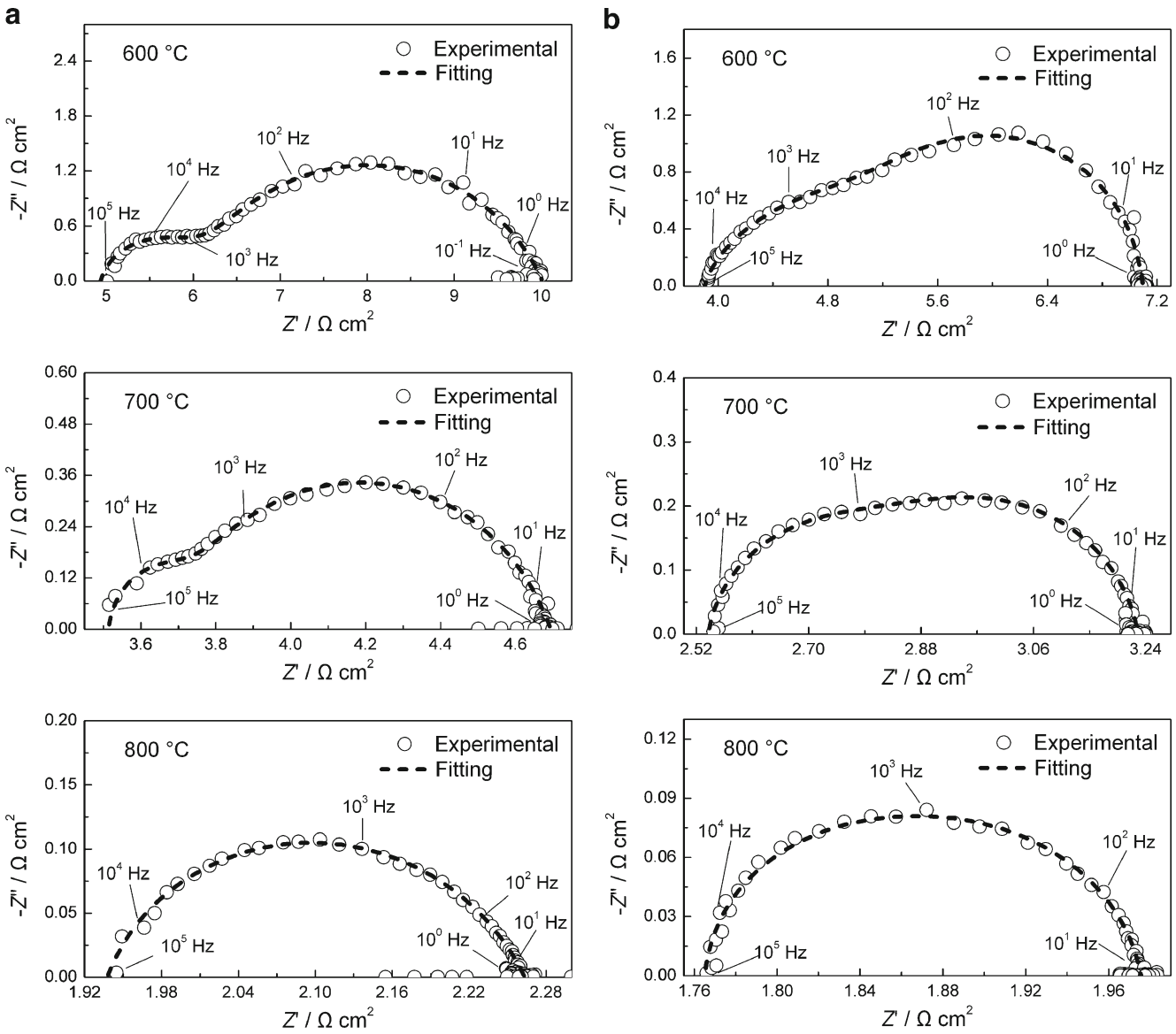

Fig. 4 Nyquist plots of **a** LN, **b** LN-LSCF, and **c** LN-SDC electrodes measured at different temperatures

Compared with the LN electrode, the LN-SDC composite electrode showed apparently reduced R_1 values at 600 °C and 650 °C, respectively. For the composite electrode, the impedance response of the charge transfer process disappeared with a further increasing in the measurement temperature. Meanwhile, the R_2 values of the composite electrode became obviously larger when compared with the LN electrode case. At an identical measurement temperature, the R_p of the composite electrode increased roughly once relative to the LN electrode. These results reveal a twofold effect of the SDC constituent on the electrode reaction. With superior oxygen-ionic conductivity, the addition of the SDC facilitated the transport of oxygen ions across the electrode/electrolyte interface, accounting for the remarkable decrease of the R_1 [9]. On the other hand, the electronic conductivity of the SDC is rather poor in the oxidizing atmosphere [30]. Thus, the addition of the SDC is unfavorable to the electron transfer process, causing an increase in R_2. The data of R_p indicate that the latter effect of the SDC is likely to be prevailing to the overall electrode polarization.

The addition of the LSCF constituent resulted in a desired change in the kinetics of the electrode reaction. No impedance response corresponding to the charge transfer process could be resolved for the LN-LSCF composite electrode over the whole measurement range. This phenomenon is believed to be mainly due to the appreciable oxygen-ionic conductivity of the LSCF. Moreover, R_2 and R_3 values of the composite electrode were obviously decreased compared with the LN electrode. This variation can be related to the

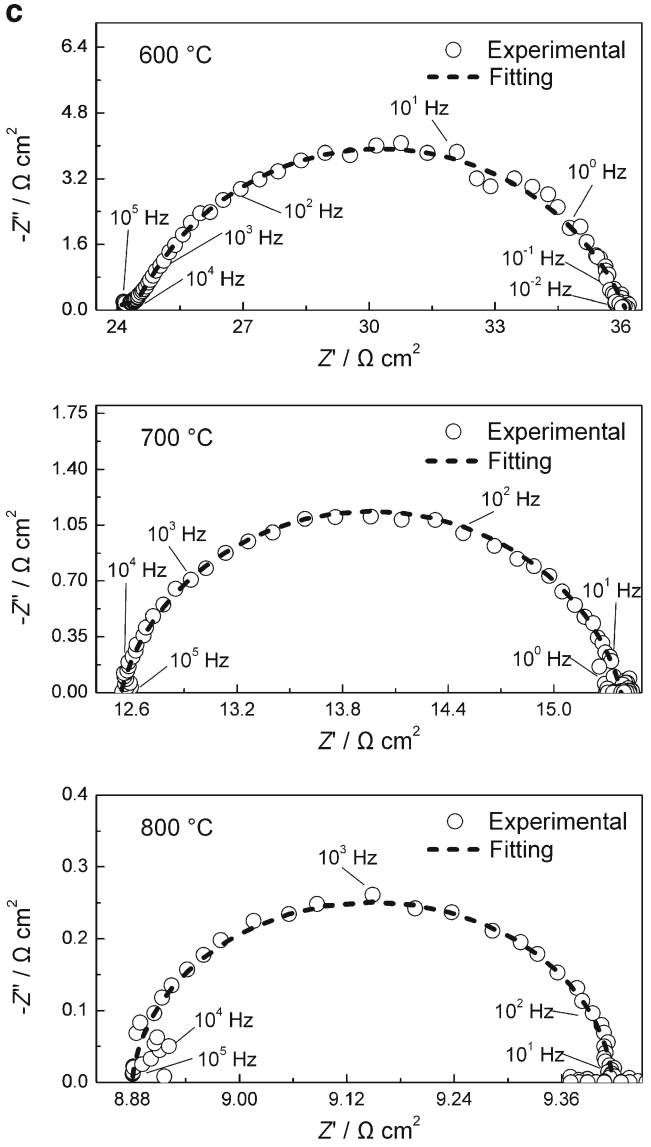

Fig. 4 (continued)

mixed conducting peculiarity of the LSCF. It is conceivable that the high electronic conductivity of the LSCF favors the electron transfer between the electrode and oxygen, leading to the decrease of the R_2. As has been well-established, the transport of oxygen ions in the LSCF occurs via oxygen vacancy mechanism. The oxygen vacancies on the surface of the LSCF can serve to be preferred sites for the adsorption and the subsequent dissociation of molecular oxygen [31]. This case is believed to be responsible for the decrease in R_3. Additionally, it was noticed that the polarization resistances of the LN electrode at high temperatures mainly came from the electron transfer process while R_2 appeared to be less prominent in the contribution toward the polarization resistances of the composite electrode at high temperatures. This comparison highlights the role of the electronic conducting component in promoting the electronic transfer

Table 1 Results of the electrochemical impedance spectra fitting for LN, LN-LSCF, and LN-SDC electrodes at different temperatures

Electrode composition	Measurement temperature, °C	R_{el}, Ω cm^2	R_1, Ω cm^2	Q_{1c}, Ω cm^2 s^{-n}	n_1	C_1, F cm^{-2}	f_1, Hz	R_2, Ω cm^2	Q_2, Ω cm^2 s^{-n}	n_2	C_2, F cm^{-2}	f_2, Hz	R_3, Ω cm^2	Q_3, Ω cm^2 s^{-n}	n_3	C_3, F cm^{-2}	f_3, Hz	R_p, Ω cm^2
LN	600	4.82	1.28	4.20×10^{-4}	0.70	1.75×10^{-5}	2987	–	–	–	–	–	3.92	5.70×10^{-3}	0.72	1.29×10^{-3}	47	5.20
	650	4.08	0.47	1.04×10^{-4}	0.80	8.69×10^{-6}	12941	–	–	–	–	–	1.91	1.78×10^{-3}	0.93	1.17×10^{-3}	122	2.38
	700	3.50	0.19	8.28×10^{-5}	1.00	8.28×10^{-5}	10120	1.00	3.68×10^{-3}	0.76	6.13×10^{-4}	341	–	–	–	–	–	1.19
	750	2.40	0.08	7.21×10^{-5}	0.99	6.38×10^{-5}	30841	0.53	3.84×10^{-3}	0.71	2.93×10^{-4}	1010	–	–	–	–	–	0.61
	800	1.89	0.04	2.11×10^{-5}	1.00	2.11×10^{-5}	187494	0.33	3.51×10^{-3}	0.71	2.36×10^{-4}	2002	–	–	–	–	–	0.37
LN-LSCF	600	3.88	–	–	–	–	–	1.58	1.52×10^{-3}	0.70	1.28×10^{-4}	789	1.65	1.28×10^{-3}	1.00	1.28×10^{-3}	71	3.23
	650	3.14	–	–	–	–	–	0.62	2.44×10^{-3}	0.71	1.75×10^{-4}	1463	0.78	1.18×10^{-3}	1.00	1.18×10^{-3}	171	1.40
	700	2.53	–	–	–	–	–	0.28	7.81×10^{-4}	0.90	3.15×10^{-4}	1792	0.40	4.15×10^{-3}	0.89	1.87×10^{-3}	208	0.68
	750	2.07	–	–	–	–	–	0.11	9.52×10^{-4}	0.96	6.64×10^{-4}	2184	0.21	4.14×10^{-3}	0.88	1.62×10^{-3}	459	0.32
	800	1.77	–	–	–	–	–	0.07	9.37×10^{-4}	0.98	8.25×10^{-4}	2558	0.13	4.11×10^{-3}	0.89	1.56×10^{-3}	747	0.20
LN-SDC	600	23.93	0.5	3.53×10^{-4}	0.68	6.00×10^{-6}	49237	11.69	2.94×10^{-3}	0.75	9.77×10^{-4}	13	–	–	–	–	–	12.19
	650	16.50	0.21	2.85×10^{-4}	0.77	1.80×10^{-5}	42505	5.39	1.72×10^{-3}	0.77	4.13×10^{-4}	71	–	–	–	–	–	5.60
	700	12.54	–	–	–	–	–	2.84	6.25×10^{-4}	0.86	2.21×10^{-4}	252	–	–	–	–	–	2.84
	750	10.25	–	–	–	–	–	1.03	4.04×10^{-4}	0.94	2.46×10^{-4}	624	–	–	–	–	–	1.03
	800	8.88	–	–	–	–	–	0.54	3.70×10^{-4}	0.96	2.53×10^{-4}	1171	–	–	–	–	–	0.54

process. The accelerated electrode processes of the composite electrode yielded a reduced electrode polarization. At each temperature, the R_p of the composite electrode was lowered by nearly onefold relative to the LN electrode. At 800 °C, the composite electrode showed a R_p of 0.20 Ω cm^2, which is very close to those (0.18 Ω cm^2) for the LSCF electrodes determined at the same temperature [32, 33].

Figure 5 shows the Arrhenius plots of R_p for the LN, LN-LSCF, and LN-SDC electrodes. The plots displayed basically a linear relation. The activation energies (E_a) of the overall electrode reaction were determined from a linear fitting of the plots. The activation energies (1.07–1.28 eV) of the three electrodes are in reasonable agreement with the literature results for oxygen reduction on the surface of mixed conducting cathodes [6, 13, 25].

Figure 6 shows the cathodic polarization curves of the LN, LN-LSCF, and LN-SDC electrodes measured at 700 °C and 800 °C, respectively. At each temperature, the LN-LSCF composite gave the lowest overpotential among the three electrodes in the case of an identical current density. At 800 °C, the LN, LN-LSCF, and LN-SDC electrodes presented overpotentials of 103, 45, and 164 mV, respectively, at a current density of 200 mA cm^{-2}. The overpotential data suggest a high electrocatalytic activity of the composite electrode, which is consistent with its low polarization resistance determined by EIS analysis. On the other hand, the overpotential value of the LN-LSCF electrode is a little larger than the result (27 mV at 200 mA cm^{-2}) of the LSCF electrode on the SDC electrolyte obtained at an identical temperature [32].

In a low overpotential region (≤20 mV), the relation of overpotential (η_{WE}) vs. current-density (I) can be expressed by the following linear equation [34]:

$$\eta_{WE} = \frac{RT}{nFi_0} I \tag{5}$$

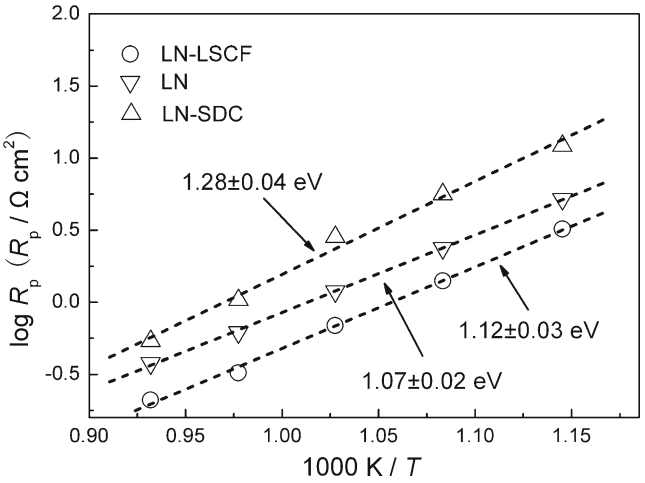

Fig. 5 Arrhenius plots for the overall polarization resistance (R_p) of LN, LN-LSCF, and LN-SDC electrodes

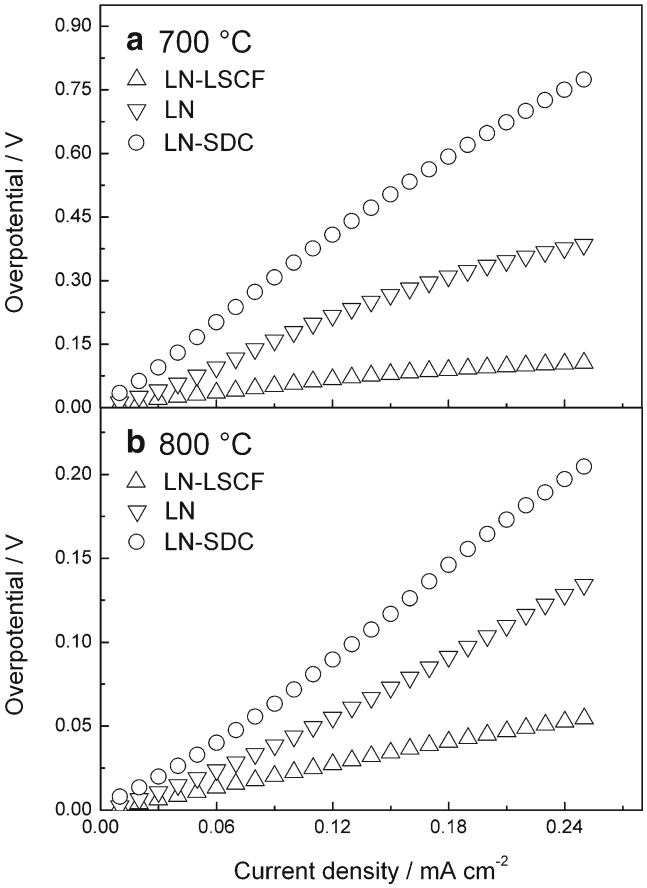

Fig. 6 Cathodic polarization curves for LN, LN-LSCF, and LN-SDC electrodes measured at **a** 700 °C and **b** 800 °C

Where i_0 is the exchange current density, n is the number of electrons involved in the electrode reaction, F is the Faraday constant, R is the gas constant, and T is the measurement temperature. The term RT/nFi_0, with a unit of ohms square centimeter, refers to the polarization resistance of the electrode reaction at an open circuit potential. The value of the term was determined from a linear fitting of the cathodic polarization curves within the low overpotential range ≤20 mV. At 800 °C, the LN, LN-LSCF, and LN-SDC electrodes showed the results of 0.41±0.01, 0.23±0.01, and 0.60±0.01 Ω cm^2, respectively. These polarization resistances are basically consistent with their counterparts (0.37, 0.20, and 0.54 Ω cm^2) determined by the EIS analysis and at the same by temperature.

Linear fitting also yielded the exchange current density i_0. At 800 °C, the exchange current densities of the LN, LN-LSCF, and LN-SDC electrodes were calculated to be 112±10, 201±10, and 77±10 mA cm^{-2}, respectively. The exchange current density is viewed as an important criterion to evaluate the kinetics of the electrode reaction [35]. The large exchange current density of the LN-LSCF electrode substantiates its superior electrocatalytic activity among the three electrodes, which agrees well with the results of the EIS analysis.

Conclusions

$La_2NiO_{4+\delta}$, 60 wt.% $La_2NiO_{4+\delta}$–40 wt.% $La_{0.6}Sr_{0.4}Co_{0.2}Fe_{0.8}O_{3-\delta}$, and 60 wt.% $La_2NiO_{4+\delta}$–40 wt.% $Ce_{0.8}Sm_{0.2}O_{1.9}$ electrodes were prepared on $Ce_{0.8}Sm_{0.2}O_{1.9}$ electrolyte substrates by screen-printing technique. The electrochemical properties of the composite electrodes were investigated in comparison with the $La_2NiO_{4+\delta}$ electrode. The charge transfer at the electrode/electrolyte interface and oxygen exchange on the electrode surface were resolved to be the main electrode processes. The surface oxygen exchange process provided a dominant contribution to the overall electrode polarization. The addition of oxygen-ionic conducting $Ce_{0.8}Sm_{0.2}O_{1.9}$ into $La_2NiO_{4+\delta}$ accelerated the charge transfer process whereas it was unfavorable to the surface oxygen exchange process due to its low electronic conductivity. By comparison, adding mixed conducting $La_{0.6}Sr_{0.4}Co_{0.2}Fe_{0.8}O_{3-\delta}$ into $La_2NiO_{4+\delta}$ was effective in promoting both the two electrode processes. Among the investigated electrodes, the $La_2NiO_{4+\delta}$–$La_{0.6}Sr_{0.4}Co_{0.2}Fe_{0.8}O_{3-\delta}$ composite electrode approached the optimum electrochemical properties. At 800 °C, the composite electrode exhibited a polarization resistance of 0.20 Ω cm^2, an overpotential of 45 mV at a current density of 200 mA cm^{-2}, together with an exchange current density of ~200 mA cm^{-2}.

Acknowledgments This work was financially supported by Natural Science Foundation of China (50572079 and A3 Foresight Program-50821140308), Ministry of Education (200804971002), Wuhan Science and Technology Bureau (200851430485), and Basic Science Research Program through the National Research Foundation of Korea (NRF) funded by the Ministry of Education, Science and Technology (2010–0002314).

References

1. Tsipis E, Kharton V (2008) J Solid State Electrochem 12(9):1039–1060
2. Kharton VV, Viskup AP, Naumovich EN, Marques FMB (1999) J Mater Chem 9(10):2623–2629
3. Skinner SJ, Kilner JA (2000) Solid State Ionics 135(1–4):709–712
4. Mauvy F, Lalanne C, Bassat JM, Grenier JC, Zhao H, Huo L, Stevens P (2006) J Electrochem Soc 153(8):A1547–A1553
5. Lalanne C, Mauvy F, Siebert E, Fontaine ML, Bassat JM, Ansart F, Stevens P, Grenier JC (2007) J Eur Ceram Soc 27(13–15):4195–4198
6. Amow G, Davidson IJ, Skinner SJ (2006) Solid State Ionics 177 (13–14):1205–1210
7. Mauvy F, Lalanne C, Fourcade S, Bassat JM, Grenier JC (2007) J Eur Ceram Soc 27(13–15):3731–3734
8. Aguadero A, Escudero MJ, Perez M, Alonso JA, Daza L (2007) J Fuel Cell Sci Technol 4(3):294–298
9. Pérez-Coll D, Aguadero A, Escudero MJ, Núñez P, Daza L (2008) J Power Sources 178(1):151–162
10. Kammer K (2009) Ionics 15(3):325–328
11. Kharton VV, Tsipis EV, Yaremchenko AA, Frade JR (2004) Solid State Ionics 166(3–4):327–337
12. Mauvy F, Lalanne C, Bassat JM, Grenier JC, Zhao H, Dordor P, Stevens P (2005) J Eur Ceram Soc 25(12):2669–2672
13. Escudero MJ, Aguadero A, Alonso JA, Daza L (2007) J Electroanal Chem 611(1–2):107–116
14. Zhao H, Mauvy F, Lalanne C, Bassat JM, Fourcade S, Grenier JC (2008) Solid State Ionics 179(35–36):2000–2005
15. Pérez-Coll D, Aguadero A, Escudero MJ, Daza L (2009) J Power Sources 192(1):2–13
16. Kharton VV, Marques FMB (2002) Curr Opin Solid State Mater Sci 6(3):261–269
17. Tsipis E, Kharton V (2008) J Solid State Electrochem 12 (11):1367–1391
18. Kharton VV, Marques FMB, Atkinson A (2004) Solid State Ionics 174(1–4):135–149
19. Huang DP, Xu Q, Zhang F, Chen W, Liu HX, Zhou J (2006) Mater Lett 60(15):1892–1895
20. Xu Q, Huang DP, Chen W, Zhang F, Wang BT (2007) J Alloys Compd 429(1–2):34–39
21. Chen M, Kim BH, Xu Q, Ahn BK, Kang WJ, Huang DP (2009) Ceram Int 35(4):1335–1343
22. Chen D, Lin Z, Zhu H, Kee RJ (2009) J Power Sources 191 (2):240–252
23. Choy KL, Charojrochkul S, Steele BCH (1997) Solid State Ionics 96(1–2):49–54
24. Østergård MJL, Clausen C, Bagger C, Mogensen M (1995) Electrochim Acta 40(12):1971–1981
25. Chen D, Ran R, Zhang K, Wang J, Shao Z (2009) J Power Sources 188(1):96–105
26. Adler SB (2004) Chem Rev 104(10):4791–4844
27. Adler SB, Lane JA, Steele BCH (1996) J Electrochem Soc 143 (11):3554–3564
28. Takeda Y, Kanno R, Noda M, Tomida Y, Yamamoto O (1987) J Electrochem Soc 134(11):2656–2661
29. Bebelis S, Kotsionopoulos N, Mai A, Rutenbeck D, Tietz F (2006) Solid State Ionics 177(19–25):1843–1848
30. Li H, Xia C, Zhu M, Zhou Z, Meng G (2006) Acta Mater 54 (3):721–727
31. Qiang F, Sun K, Zhang N, Zhu X, Le S, Zhou D (2007) J Power Sources 168(2):338–345
32. Zhao K, Xu Q, Huang DP, Chen M, Kim BH (2011) Ionics 17 (3):247–254
33. Qiang F, Sun KN, Zhang NQ, Le SR, Zhu XD, Piao JH (2009) J Solid State Electrochem 13(3):455–467
34. Fu C, Sun K, Zhang N, Chen X, Zhou D (2007) Electrochim Acta 52(13):4589–4594
35. Liu B, Zhang Y, Zhang L (2009) Int J Hydrog Energy 34(2):1008–1014